Design of W-type Index Chalcogenide Fiber for Highly Coherent Mid-IR Supercontinuum Generation

M A Khamis, R Sevilla and K Ennser

***Abstract*—This paper presents the design of a W-type index chalcogenide fiber for mid-infrared beyond 10µm. The main advantages of the W-type index fiber are the possibility to control the chromatic dispersion with a larger possible core area for single-mode operation compared to a common step-index fiber and to enhance the fiber nonlinearity. Our fiber design consists of $Ge_{15}Sb_{15}Se_{70}$ glass core, $Ge_{20}Se_{80}$ glass inner cladding and $Ge_{20}Sb_5Se_{75}$ glass outer cladding. The optical mode distribution of the chalcogenide fiber is numerically calculated by a finite element method based on edge element analysis. With 6-µm core diameter and 12-µm inner cladding diameter, the proposed fiber design exhibits flat anomalous dispersion in the wavelength range (4.3-6.5µm) with a peak of about 7ps/(nm·km). Also, it offers a high nonlinear coefficient of 0.12 $W^{-1}m^{-1}$ at a pump wavelength of 6.3 µm. The simulation results show that our proposed fiber design provides a highly coherent Mid-IR SC extending from 3.7 to 12 µm pumped at low peak pump power of 1kW.**

***Index Terms*—Nonlinear optical materials and devices, supercontinuum generation, ultrafast nonlinear optics.**

I. INTRODUCTION

Considerable efforts have been devoted to the mid-infrared (Mid-IR) coherence sources because of the potential applications of these sources in spectroscopy, metrology, few-cycle pulse compression and optical coherence tomography [1-3]. One potential enabling technology for a Mid-IR coherent light source is to explore the supercontinuum (SC) generation in the optical fiber [4]. To achieve a wide Mid-IR SC generation, it is more efficient to pump the nonlinear fiber in its anomalous dispersion regime. At this regime, the pulse spectrum is broadened through soliton effects [5,6] However, these solitons are very sensitive to laser noise and produce fluctuations in the phase and intensity of the spectrum from one pulse to the next that ultimately lead to poor spectral coherence. There are two important factors to overcome this limitation and achieve high coherence of Mid-IR SC generation [7] First, it is necessary to adjust the chromatic dispersion to a small absolute value in the Mid-IR region. Second, the required nonlinear effects are achieved by using a small effective mode diameter and by employing materials with a large third-order nonlinear refractive index (n_{NL}). It is worth noting that properties such as the pulse duration and the position of the pump wavelength spectral to fiber zero dispersion wavelength (ZDW) must be taken into consideration. One promising way to achieve these conditions is to employ the step-index fiber (SIF) for SC generation [8]. This type of fiber possesses the benefit of high optical damage threshold, good mechanical robustness and high-power handling capacity [9]. However, it is challenging to tailor the chromatic dispersion in standard SIF. Additionally, because of a big core diameter and loose mode confinement, the nonlinearity in a SIF is weaker compared to a microstructured optical fiber.

An alternative approach to control the chromatic dispersion is by applying W-type index fiber profile. The advantages of such a double-clad fiber are a tight confinement mode, a flattened dispersion profile, more flexibility to control the locations of the ZDWs than in that SIF, and a higher possible V-parameter (V = 3.8) as compared to (2.405) at SIF. This large value of the V-parameter enables the enlargement of the core diameters whilst maintaining the single mode operation, resulting in lower coupling losses [10]. Also, this fiber type can be fusion spliced to standard SIF therefore it is suitable for an all-fiber system. The investigation of tellurite W-type index structure has been already considered for Mid-IR SC (2-5 µm) [10-12]. However, this type of fiber remains unexplored for chalcogenide based Mid-IR SC.

The Ge-Sb-Se glass system has been studied for many years [13]. This glass exhibits lower vapour pressure and better transmission between 10µm to 14µm as compared to the Ge-As-Se system. This is because of the Antimony (Sb) assists the shifting of the multi-phonon edge to longer wavelengths. In addition, it has relatively large n_{NL} and high laser damage threshold of about 3674 GW/cm^2 which is more than twice times larger compared to As_2Se_3 glass [14-16].

Finite element method (FEM) is the most efficient approach to design a waveguide on its 2D cross-section [17]. This technique can be used to analyze waveguides with complex geometries such as a photonic crystal fiber (PCF) [18], a nanowire [19] and a double cladding fiber [20]. In this study, FEM based edge elements are used to evaluate the properties of W-type index fiber, such as the effective index, the chromatic dispersion and the effective mode area. Contrary to traditional nodal finite elements, the edge elements considered here avoid the presence of spurious (non-physical) modes. In

Submitted on May 18, 2018. This work was supported by the High Committee for Education Development in Iraq (HCED).

M. A. Khamis, R. Sevilla and K. Ennser are with College of Engineering, Swansea University, Bay Campus, Fabian Way, Swansea, SA1 8EN, Wales, United Kingdom. M. A. Khamis is also with Baqubah Technical Institute, Middle Technical University, Baghdad, Iraq. (email:805172@swansea.ac.uk).

This article has been accepted for publication in a future issue of this journal, but has not been fully edited. Content may change prior to final publication. Citation information: DOI 10.1109/JLT.2018.2873589, Journal of Lightwave Technology

addition, edge elements lead to an easy implementation of boundary conditions at material interfaces [21,22]. However, the required number of floating point operations per conjugate gradient operation and the storage requirements in linear edge elements are more than twice as expensive to linear nodal elements [23].

This work investigates the design of a W-type index chalcogenide fiber for SC generation. Our fiber design has a high nonlinear coefficient, flattened dispersion profile and a tight confinement of the mode within the core. In addition, the numerical simulations of SC show that our fiber design exhibits highly coherence Mid-IR SC extending from 3.7 to 12 μm when it is pumped with femtosecond laser pulses with peak power of 1kW. To the best of our knowledge, this work produced the broadest highly coherent Mid-IR SC pumped with low peak power.

II. FEM FORMULATION OF THE FIBER GUIDED MODE

FEM based edge elements are employed to compute the effective index of the proposed W-type fiber. Contrary to other finite element methods, the edge elements considered here lead to spurious-free solutions and a natural imposition of the boundary conditions at material interfaces. We use the vector FEM approach that provides immunity from having spurious modes. To compute the continuous spectrum of the proposed fiber, the structure is enclosed by an electrical wall and the vector wave equation is solved using edge finite elements. The formulation considered here considers the wave equation for the electric (**E**) field, namely [21]

$$\nabla\times\left(\frac{1}{\mu_r}\nabla\times\mathbf{E}\right)-k_0^2\varepsilon_r\mathbf{E}=0 \tag{1}$$

where k_0 is the free space wave number, ε_r and μ_r are the permittivity and permeability of the materials in the waveguide, respectively. By splitting the electric field into its transverse (subscript t) and longitudinal (subscript z) the following two decoupled equations are obtained

$$\nabla_t\times\left(\frac{1}{\mu_r}\nabla_t\times\mathbf{E}_t\right)+\frac{1}{\mu_r}\left(k_z^2\nabla_t\mathrm{E}_z\right)+k_z^2\mathbf{E}_t=k_o^2\varepsilon_r\mathbf{E}_t \tag{2}$$

$$-\frac{1}{\mu_r}\left(\nabla_t\cdot\left(\nabla_t\mathrm{E}_z+\mathbf{E}_t\right)\right)=k_o^2\varepsilon_r\mathrm{E}_z \tag{3}$$

where k_z is the propagation constant. The finite element discretization leads to a generalized eigenvalue problem that is solved to obtain the propagation constant k_z or the eigenvalues. The effective refractive index n_{eff} is obtained by using the relation:

$$n_{eff}=\frac{k_z}{k_o} \tag{4}$$

III. NONLINEAR AND DISPERSION CHARACTERIZATION

The chromatic dispersion D(λ) is calculated from the effective index n_{eff} values versus wavelength λ by the following formula [22]

$$D(\lambda)=-\frac{\lambda}{c}\frac{\partial^2\,\mathrm{Re}\left(n_{eff}(\lambda)\right)}{\partial\lambda^2} \tag{5}$$

where c is the velocity of light in vacuum and $\mathrm{Re}(n_{eff})$ is the real part of fundamental mode effective index. Another important parameter is the effective mode area which represents the effective area of propagating mode in the W-type index fiber. The effective mode area equation is given by:

$$A_{eff}=\frac{\left(\int\int_{-\infty}^{+\infty}|\mathbf{E}(x,y)|^2\,dxdy\right)^2}{\int\int_{-\infty}^{+\infty}|\mathbf{E}(x,y)|^4\,dxdy} \tag{6}$$

Here, **E** (x,y) is the optical field distribution across the fiber cross-section which is evaluated from the FEM solution of eq. 2 and 3. Then, the integrals are computed over the computational domain. The nonlinear parameter can be expressed as:

$$\gamma\left(W^{-1}m^{-1}\right)=\frac{2\pi n_{NL}}{\lambda A_{eff}} \tag{7}$$

From eq. 7, the nonlinearity coefficient γ can be controlled via two factors, nonlinear refractive index (n_{NL}) and A_{eff}.

IV. DESIGN OF W-TYPE INDEX CHALCOGENIDE FIBER

A W-type fiber consists of three different refractive index materials. The core has the largest refractive index of the three, and the inner cladding index is the lowest. Our proposed fiber is composed of core $Ge_{15}Sb_{15}Se_{70}$ (n_1), inner cladding $Ge_{20}Se_{80}$ (n_2) and outer cladding $Ge_{20}Sb_5Se_{75}$ (n_3) as shown in fig. 1, r_1 and r_2 are the core and inner cladding radius, respectively. The wavelength dependent linear refractive indices of chalcogenide $Ge_{15}Sb_{15}Se_{70}$, $Ge_{20}Se_{80}$ and $Ge_{20}Sb_5Se_{75}$ are obtained from [15,24] and shown in fig. 2.

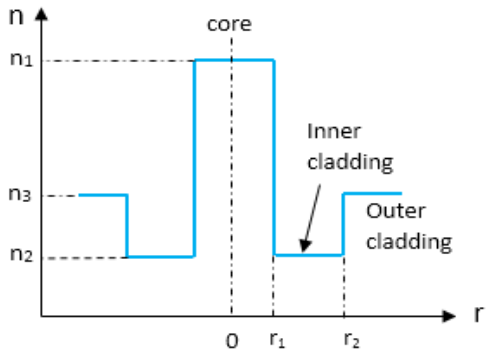

Fig. 1. Refractive index profile of W-type index chalcogenide fiber.

The V-parameter for the W-type index chalcogenide fiber can be written as [8]:

$$V=\frac{2\pi r_1}{\lambda}\times NA=\frac{2\pi r_1}{\lambda}\sqrt{n_1^2-n_3^2} \tag{8}$$

This article has been accepted for publication in a future issue of this journal, but has not been fully edited. Content may change prior to final publication. Citation information: DOI 10.1109/JLT.2018.2873589, Journal of Lightwave Technology

where λ is the wavelength, NA is the numerical aperture, r_1 is the core radius. The W-type index has a larger core area for single-mode operation due to its higher V-parameter (V = 3.8) than the conventional SIF. The advantage of a larger possible core diameter is the reduction of the coupling losses while still operating under single-mode condition.

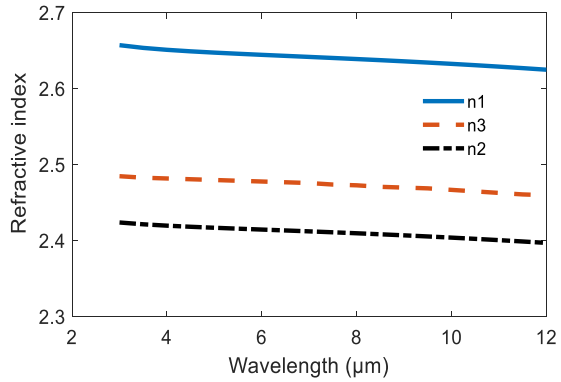

Fig. 2. The refractive index for the core, inner and outer cladding versus wavelength for synthesized $Ge_{15}Sb_{15}Se_{70}$, $Ge_{20}Se_{80}$ and $Ge_{20}Sb_5Se_{75}$ glasses [15,24].

However, a smaller effective refractive index of the core and inner cladding may lead to a leakage of the mode power into the outer cladding and therefore resulting in a catastrophic loss for the mode. This effect can be present when the mode field radius and the operating wavelength become too large. Hence, an effective cutoff wavelength λ_f exists and occurs at a V-parameter [10] of around 1.4. From the above two conditions, the operating wavelength must be between λ_f and the single-mode cutoff wavelength (λ_c), that is, $\lambda_c < \lambda < \lambda_f$.

In our chalcogenide fiber, we optimize the core diameter to achieve the two above conditions in the range of operating wavelengths between 4.8 and 12μm. The calculation of V-parameter using eq. 8 is shown in fig. 3. The results show that a suitable core diameter is 6 μm to keep the fiber under the single-mode boundary in the chosen range.

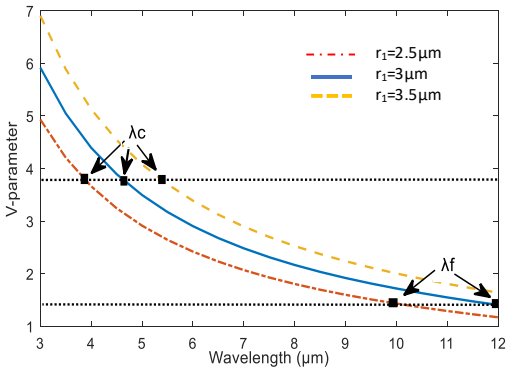

Fig. 3. Calculated V-parameter for the W-type index chalcogenide fiber at core radiuses 2.5μm, 3μm and 3.5μm with single-mode cutoff-wavelengths at λ_c, and cutoff-wavelengths due to leakage losses at λ_f. The single-mode boundary at V = 3.8 and the leakage boundary at V = 1.4 are marked with black dotted lines.

The guiding properties of the designed W-type index fiber are analysed by calculating the guided modes using our FEM software based on edge elements. We computed the propagation constant at the operating wavelength of 6.3 μm with a series of three successively refined finite element meshes as shown in Table I. The element size of each new mesh refinement is half of the previous mesh. The results illustrate how the computed value of the propagation constant converges as the mesh is refined. In the remaining of the paper the value of the propagation constant computed in the second mesh is considered as the accuracy provided is considered enough for the subsequent calculations.

TABLE I
THE COMPUTED PROPAGATION CONSTANT AT THE OPERATING WAVELENGTH OF 6.3 μm WITH A SERIES OF THREE SUCCESSIVELY REFINED FINITE ELEMENT MESHES.

Number of mesh elements	Propagation constant (k_z)
660	2.554193e+06
2640	2.561344e+06
10560	2.561348e+06

Figure 4 illustrates the chromatic dispersion characteristic of our reported fiber structure at 6μm of core diameter and different inner cladding diameters. As shown in fig. 4, there are two zero dispersion wavelengths (ZDWs) and the first ZDWs remain nearly fixed for different inner cladding diameters and are located at around 4.3μm. The second ZDWs increase with the inner cladding diameter and are located at 6μm, 6.5μm and 7μm with inner cladding diameter of 9μm, 12μm and 18μm, respectively.

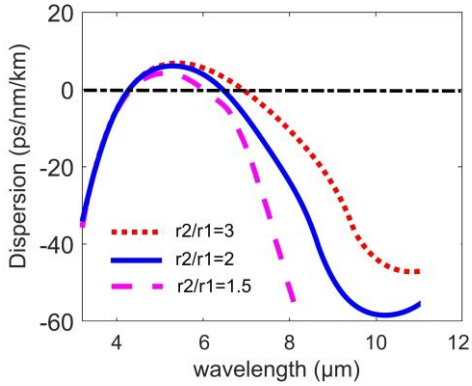

Fig. 4. Calculated dispersion profiles versus wavelength for W-type index chalcogenide fiber.

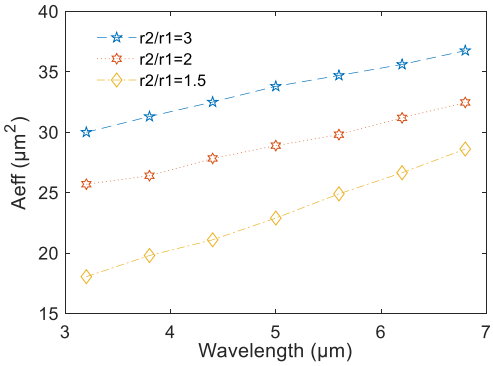

Fig. 5. Calculated effective area versus wavelength for W-type index chalcogenide fiber.

Between these two ZDWs the fiber exhibits a low and flat anomalous dispersion. Moreover, this fiber structure shifts ZDWs to longer wavelengths. In addition, the calculated spectral variation of the effective mode area is shown in fig. 5. It is clearly observed that the effective mode area increases with the inner cladding diameter.

Based on the obtained results, we select the inner cladding diameter of 12 µm (r_2/r_1=2), and a pump wavelength of 6.3µm, which is near the second ZDWs in the anomalous dispersion regime. At this pump wavelength, the dispersion is D =3.24ps/(nm·km) and the effective area equals 32µm^2. Typically, the $Ge_{15}Sb_{15}Se_{70}$ glass offers a high nonlinear refractive index of about 10.34m^{2}W^{-1} at the wavelength of 1.55 µm [25]. We assume that the nonlinear refractive index n_{NL} at 6.3 µm to be about 30% of that value at 1.55 µm as suggested in [22] resulting in a nonlinear parameter of about 0.12 W^{-1} m^{-1}. This nonlinear parameter is two times higher than previously reported step-index fiber [8]. As a result, the proposed W-type index chalcogenide structure ensures single-mode propagation, which improves the nonlinearity, flattened anomalous dispersion profile and low losses due to a tight confinement of the mode within the core.

V. SUPERCONTINUUM GENERATION

The evolution of the SC spectrum can be described by the numerical solution to the subsequent generalized nonlinear Schrödinger equation (GNLSE) for the output pulse envelope A(z,t). The change in the pulse envelope A(z,t) during propagation along an optical fiber can be described by [26]:

$$\frac{\partial A}{\partial z}+\frac{\alpha}{2}A-\sum_{q=1}^{10} i^{q-1}\frac{\beta_q}{q!}\frac{\partial^q A}{\partial t^q}=i\gamma\left(1+\frac{i}{\omega_o}\frac{\partial}{\partial t}\right)\times\left[A(z,t)\int_{-\infty}^{+\infty}R(t')\left|A(z,t-t')\right|^2dt'\right] \quad (9)$$

where α is the transmission loss of the fiber which is equal to 5dB/m at the pump wavelength of 6.3 µm [15], ω_0 is the center angular frequency of the pulse, *t* and *z* are the time variable and the spatial coordinate along the fiber, γ is the nonlinear coefficient, β_q represents the q–th order dispersion parameter. The response function R(t), including both instantaneous electronic and delayed Raman contributions, can be expressed by:

$$R(t)=(1-f_R)\delta(t)+f_R h_R(t) \quad (10)$$

Here, δ(t) is the Dirac delta function and f_R is the fractional contribution of the delayed Raman response function h_R(t). The Raman response function can be approximately expressed as:

$$h_R(t)=\frac{\left(\tau_1^2+\tau_2^2\right)}{\tau_1\tau_2^2}\exp(-t/\tau_2)\sin(t/\tau_1) \quad (11)$$

The parameters τ_1 and τ_2 are two adjustable parameters and are chosen to provide a good fit to the actual Raman-gain spectrum. In our simulations, the hyperbolic secant pulse is used as an input pulse which expressed as:

$$A(0,t)=\sqrt{p_o}\,\mathrm{sec}h\left(\frac{t}{T_o}\right)=\sqrt{\frac{|\beta_2|}{\gamma}}\frac{N}{T_o}\mathrm{sec}h\left(\frac{t}{T_o}\right) \quad (12)$$

where p_o is the peak pulse power, T_o =T_{FWHM}/1.763, β_2 is the group velocity dispersion (GVD) parameter, and N is the soliton order.

The modulus of the complex degree of first order coherence is calculated over a finite bandwidth at each wavelength in the SC as [26,27]:

$$\left|g_{12}^{(1)}(\lambda)\right|=\left|\frac{\left\langle\mathbf{E}_1^*(\lambda)\mathbf{E}_2(\lambda)\right\rangle}{\sqrt{\left\langle\left|\mathbf{E}_1(\lambda)\right|^2\right\rangle\left\langle\left|\mathbf{E}_2(\lambda)\right|^2\right\rangle}}\right| \quad (13)$$

where $\mathbf{E_1}(\lambda)$ and $\mathbf{E_2}(\lambda)$ are the electric field associated with different SC pulse realizations, the angle brackets denote an ensemble average. We have performed each simulation with different realization of an input shot noise seed of one photon per mode with random phase in each spectral discretization bin [26]. The input noise amplitude can be expressed as:

$$A_{0ppm}(\omega)=\sqrt{\frac{h\omega}{T_{span}}}\exp\left(i2\pi\phi(\omega)\right) \quad (14)$$

Here, ω is the pulsation, h is the Planck constant, T_{span} is the temporal window used in our simulations and ϕ(ω) is a uniformly distributed random phase in the interval [0,2π]. A_{0ppm} (ω) is then inverse Fourier transformed to obtain $A_{0ppm}(t)$ which is added to the input field described in eq. 12.

VI. RESULTS AND DISCUSSION

The Split-Step Fourier Method is applied to solve the Non-Linear Schrödinger Equation. The simulations are carried out with a hyperbolic secant input pulse of a 330-fs pulse duration (FWHM) launched in the W-type index fiber at 6.3 µm. We choose the pump wavelength to reduce the impact of O-H absorption in the fiber loss. The pulse duration is selected to achieve relative high soliton number to enhance the SC generation and reduce the required peak pump power. The noise is included by adding to the input pulse one random phase photon per mode in the frequency domain. To calculate the degree of the first-order coherence, we apply the ensemble average to the results of 20 simulations of different random quantum noise of the input pulses to produce 190 Mid-IR SC pairs [7].

Firstly, we set the fiber length to 20cm and vary the peak pump power. The normalized intensity and degree of the first order coherence are drawn in fig. 6,7,8 and 9 for 500W, 1kW, 2kW and 3kW, respectively. The considered chalcogenide material with similar diameter has been experimentally demonstrated to tolerated a pump power of 6.5kW without damage [15]. We have observed that a highly coherent Mid-IR SC occurs in the range between 3.7 to 12 µm at a peak pump power of 1kW. For higher peak powers the SC spectrum continues broadening at the expenses of losing the coherence.

This article has been accepted for publication in a future issue of this journal, but has not been fully edited. Content may change prior to final publication. Citation information: DOI 10.1109/JLT.2018.2873589, Journal of Lightwave Technology

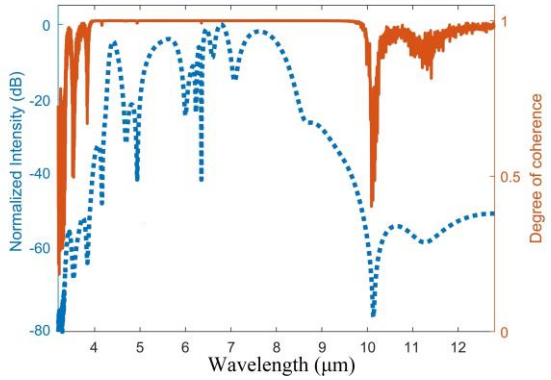

Fig. 6. Normalized intensity (blue and dashed curve, left axis) and degree of the first-order coherence (red curve, right axis) in the W-type index fiber with 500W of peak pump power for a fiber length of 20cm.

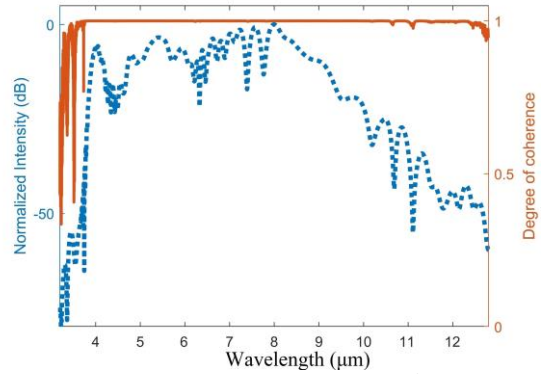

Fig. 7. Normalized intensity (blue and dashed curve, left axis) and degree of the first-order coherence (red curve, right axis) in the W-type index fiber with 1kW of peak pump power for a fiber length of 20cm.

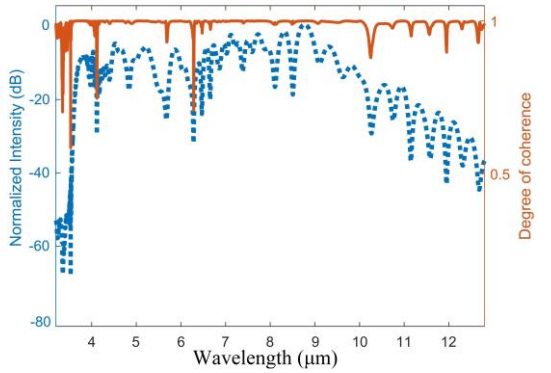

Fig. 8. Normalized intensity (blue and dashed curve, left axis) and degree of the first-order coherence (red curve, right axis) in the W-type index fiber with 2kW of peak pump power for a fiber length of 20cm.

To give more insight on the SC generation process Fig. 10 and 11 illustrate the simulated spectral and temporal evolution in W-type index chalcogenide fiber at a peak pump power of 1kW. The calculated nonlinear length ($L_{NL} = 1/\gamma P_0$) is 8.3 × 10^{-3} m. The calculated value of the dispersion length ($L_D = T_0^2/\beta_2$) is 1.345m. Thus, the value of the soliton order ($N = \sqrt{L_D/L_{NL}}$) equals to 12.7. It is clearly seen from fig. 10 that the intensity spectra broaden with the pump power due to increase in the soliton number (N). However, the increase of pump power leads to several deep dips in the first-order coherence and drop the coherence due to its dependence with soliton fission and modulation instability processes [25].

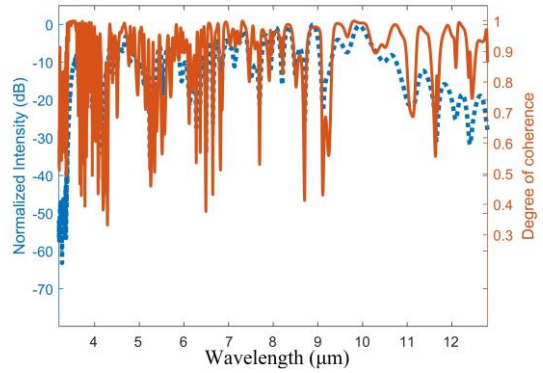

Fig. 9. Normalized intensity (blue and dashed curve, left axis) and degree of the first-order coherence (red curve, right axis) in the W-type index fiber with 3kW of peak pump power for a fiber length of 20cm.

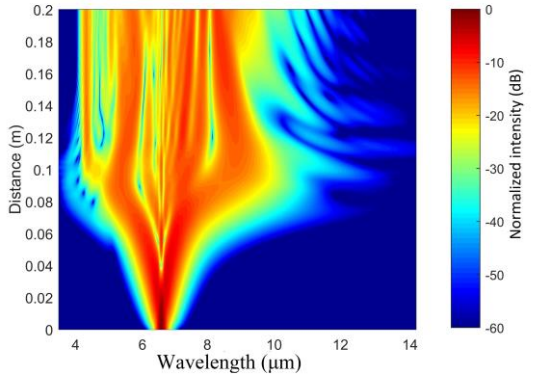

Fig. 10. Simulated spectral evolution in the W-type index fiber when it is pumped with 330-fs laser pulses of 1-kW peak power at 6.3μm and a fiber length of 20 cm.

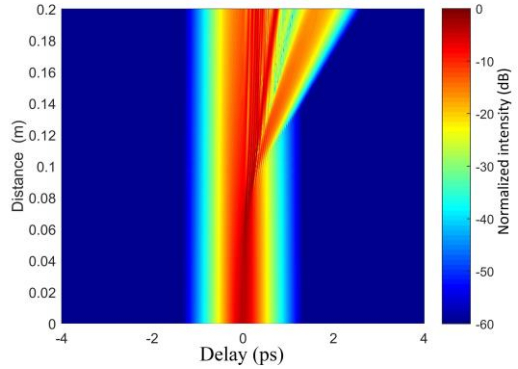

Fig. 11. Simulated temporal evolution in the W-type index fiber when it is pumped with 330-fs laser pulses of 1-kW peak power.

The next step of the investigation is to find the dependence of the intensity and coherence spectra of the Mid- IR SC with respect to the fiber length and the pulse durations. Figure 12 and 13 show the SC broadening and the coherence spectra for different fiber length of 30cm and 50cm. We notice the SC broadening is reduced with the fiber length due to the fiber loss. Also, the first-order coherence drops with the pump fiber length due to fiber dispersion accumulation as suggested in [28].

This article has been accepted for publication in a future issue of this journal, but has not been fully edited. Content may change prior to final publication. Citation information: DOI 10.1109/JLT.2018.2873589, Journal of Lightwave Technology

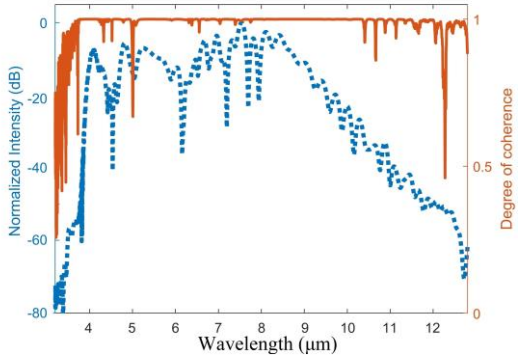

Fig. 12. Normalized intensity (blue and dashed curve, left axis) and degree of the first-order coherence (red curve, right axis) in the W-type index fiber with 30cm of fiber lengths for a peak pump power of 1kW.

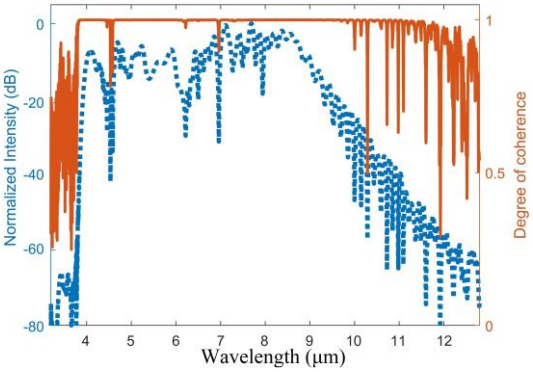

Fig. 13. Normalized intensity (blue and dashed curve, left axis) and degree of the first-order coherence (red curve, right axis) in the W-type index fiber with 50cm of fiber lengths for a peak pump power of 1kW.

Figure 14 and 15 depict the intensity and coherence spectra of the Mid-IR SC at different pulse durations. We choose the pulse duration at values that we can see a clear effect on the coherence spectra and set the peak pump power to 1 kW for 20-cm fiber length. Despite a comparable intensity in all pulse durations is observed, the degree of the first order coherence reduces with pulse durations. This is because the effects of modulation instability are reduced with shorter pulse duration when the pump power and fiber length are fixed.

In fact, the value of soliton number in the anomalous regime should be less than the condition value (N<<16) to ensure a high level of SC coherence [29]. From the simulations, the increase in pulse duration over 330fs and/or the peak pump power over 1kW degrades the pulse temporal coherence.

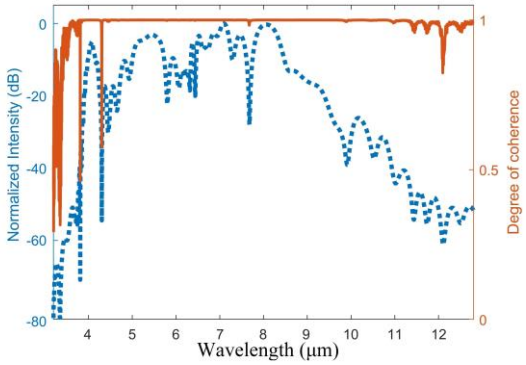

Fig. 14. Normalized intensity (blue and dashed curve, left axis) and degree of the first-order coherence (red curve, right axis) in the W-type index fiber with pulse durations of 387.8fs (FWHM) for a pump power of 1kW and a fiber length of 20cm.

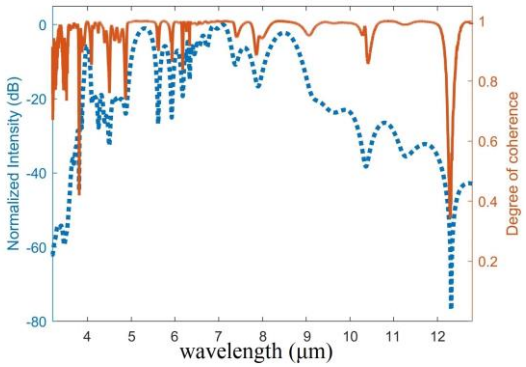

Fig. 15. Normalized intensity (blue and dashed curve, left axis) and degree of the first-order coherence (red curve, right axis) in the W-type index fiber with pulse duration 564fs (FWHM) for a pump power of 1kW and a fiber length of 20cm.

VII. Conclusions

This paper presents a design of a W-type index chalcogenide fiber for Mid-IR SC beyond 10μm. Our fiber design consists of $Ge_{15}Sb_{15}Se_{70}$ glass core, $Ge_{20}Se_{80}$ glass inner cladding and $Ge_{20}Sb_5Se_{75}$ glass outer cladding. The optical mode distribution of the chalcogenide fiber is simulated by a finite element method based on edge elements. With 6-μm core diameter and 12-μm inner cladding diameter, the proposed fiber design exhibits flat anomalous dispersion in the wavelength range (4.3-6.5μm) with a peak of about 7ps/(nm·km). The position of the second ZDW can be easily and precisely controlled by the inner cladding size. The larger the inner cladding diameter, the longer will be the zero-dispersion wavelength. However, the increase of the inner cladding diameter leads also to an increase of the effective mode area and therefore a smaller fiber nonlinear coefficient. The proposed design is more suitable for a pump wavelength at 6.3μm which is located between two ZDWs and it exhibits a low anomalous dispersion.

The simulation results show that our proposed fiber design provides a highly coherent Mid-IR SC extending from 3.7 to 12 μm pumped at 1kW. To the best of our knowledge, this work proposes the broadest highly coherent Mid-IR SC under a low peak pump power. The value of soliton number in the anomalous regime should be less than the condition value (N<<16) to ensure a high level of SC coherence.

The proposed broadband SC source is highly applicable in spectroscopy, metrology and optical coherence tomography.

REFERENCES

[1] A. Schliesser, N. Picqué, T W. Hänsch, "Mid-infrared frequency combs," *Nature Photon*., vol. 6, pp.440-449, 2012.

[2] R. Su, M. Kirillin, E.W. Chang, E. Sergeeva, S.H. Yun, L. Mattsson, "Perspectives of mid-infrared optical coherence tomography for inspection and micrometrology of industrial ceramics," *Opt. Exp*., vol. 22, pp. 15804–15819, 2014.

[3] F. C. Cruz, D.L. Maser, T. Johnson, G. Ycas, A. Klose, F.R. Giorgetta, I. Coddington, S.A. Diddams, "Mid-infrared optical frequency combs based on difference frequency generation for molecular spectroscopy," *Opt. Exp.*, vol. 23, 26814, 2015.

[4] K. Nagasaka et al., "Mid-infrared supercontinuum generation in chalcogenide multi-step index fibers with normal chromatic dispersion," *SPIE*, vol. 10100, pp. 1010021, 2017.

[5] C. R. Petersen et al., "Mid-Infrared Supercontinuum Covering the 1.4–13.3 lm Molecular Fingerprint Region Using Ultra-High NA Chalcogenide Step-Index Fibre," *Nat. Photonics*, vol. 8, pp. 830–4, 2014.

[6] U Møller et al., "Multi-milliwatt mid-infrared supercontinuum generation in a suspended core chalcogenide fiber," *Opt. Exp.*, vol. 23, pp. 3282-3291, 2015.

[7] K. Nagasaka et al., "Numerical investigation of highly coherent mid-infrared supercontinuum generation in chalcogenide double-clad fiber," *Opt. Fiber Technol*., vol. 36, pp. 82–91, 2017.

[8] T. Cheng et al., "Mid-infrared supercontinuum generation spanning 2 to 15 μm in a chalcogenide step-index fiber," *Opt. Lett*., vol. 41, pp. 2117 ,2016.

[9] A. Ben Khalifa, A. Ben Salem, R. Cherif, and M. Zghal, "Mid-infrared supercontinuum generation in multimode step index chalcogenide fiber," *SPIE*, vol. 9958, pp. 99580, 2016.

[10] S. Kedenburg et al., "Solitonic supercontinuum of femtosecond mid-IR pulses in W-type index tellurite fibers with two zero dispersion wavelengths," *APL Photonics*, vol.1, pp. 86101, 2016.

[11] C. Wei, X. Zhu, R. A. Norwood, F. Song, and N. Peyghambarian, "Numerical investigation on high power mid-infrared supercontinuum fiber lasers pumped at 3μm," *Opt. Exp*., vol. 21, pp. 29488, 2013.

[12] R. Thapa et al., "Mid-IR supercontinuum generation in ultra-low loss, dispersion-zero shifted tellurite glass fiber with extended coverage beyond 4.5 μm," *Proc. SPIE*, vol. 8898, Technologies for Optical Countermeasures X; and High-Power Lasers 2013: Technology and Systems**,** pp. 889808, 2013.

[13] P. Klocek and L. Colombo, "Index of refraction, dispersion, bandgap and light scattering in GeSe and GeSbSe glasses," *J. of Non-Crystalline Solids*, vol. 93, pp. 1–16, 1987.

[14] H. Ou et al., "Ultrabroad supercontinuum generated from a highly nonlinear Ge–Sb–Se fiber," *Opt. Lett*., vol. 41, pp. 3201, 2016.

[15] B. Zhang *et al.*, "High Brightness 2.2–12 μm Mid-Infrared Supercontinuum Generation in a Nontoxic Chalcogenide Step-Index Fiber," *J. Am. Ceram. Soc*., vol. 99, no. 8, pp. 2565–2568, 2016.

[16] J. H. Butterworth et al., "Towards mid-infrared supercontinuum generation: Ge-Sb-Se mid-infrared step-index small-core optical fiber," *SPIE BIOS*, vol. 8938, pp. 89380, 2014.

[17] B. M. A. Rahman, "Finite Element Analysis of Optical Waveguides", Progress In Electromagnetics Research, PIER 10, 187-216 (1995).

[18] M. A. Khamis, R. Sevilla and K. Ennser, "Large Mode Area Pr^{3+}-Doped Chalcogenide PCF Design for High Efficiency Mid-IR Laser," in *IEEE Photonics Technology Letters*, vol. 30, no. 9, pp. 825-828, 1 May1, 2018.

[19] M. R. Karim, B. M. A. Rahman, and G. P. Agrawal, "Dispersion engineered $Ge_{11.5}As_{24}Se_{64.5}$ nanowire for supercontinuum generation: A parametric study," Opt. Express 22, 31029-31040 (2014).

[20] K. Nagasaka *et al*., "Supercontinuum generation in the normal dispersion regime using chalcogenide double-clad fiber," *Appl. Phys. Express*, vol. 10, no. 3, 2017.

[21] G. Pelosi, R. Coccioli, and S. Selleri, "Microwave Guidance Structure: characterization" in Quick Finite Elements for Electromagnetic Waves, 2'nd ed. *ARTECH HOUSE*, pp. 59-82, 2009.

[22] M. A. Khamis, R. Sevilla, K. Ennser, "Numerical investigation on W-type index chalcogenide fiber based MIR supercontinuum generation", *Proc. SPIE*, vol. 10681, Micro-Structured and Specialty Optical Fibres V, pp.106810V, 2018.

[23] G. Murr, "Edge Elements, their Advantages and their Disadvantages," *IEEE Trans. Magn.*, vol. 30, no. 5, pp. 3552–3557, 1994.

[24] L. Chen et al., "Third-order nonlinearity in Ge-Sb-Se glasses at mid-infrared wavelengths," *Mater. Res. Bull*., vol. 70, pp. 204–208, 2015.

[25] T. Wang et al., "Systematic z-scan measurements of the third order nonlinearity of chalcogenide glasses," *Opt. Mater. Exp*., vol. 4, pp. 1011, 2014.

[26] J. M. Dudley and S. Coen, "Coherence properties of supercontinuum spectra generated in photonic crystal and tapered optical fibers*," Opt. Lett.*, vol. 27, pp. 1180, 2002.

[27] C. Ciret and S.P. Gorza, "Generation of ultrabroadband coherent supercontinuum in tapered and dispersion managed silicon nanophotonic waveguides" *J. Opt. Soc. Am. B*, vol. 34, pp. 1156, 2017.

[28] A. M. Heidt, "Pulse preserving flat-top supercontinuum generation in all-normal dispersion photonic crystal fibers," J. Opt. Soc. Am. B 27, 550-559 (2010).

[29] J. M. Dudley, G. Genty, and S. Coen, "Supercontinuum generation in photonic crystal fiber," Rev. Mod. Phys. 78, 1135–1184 (2006).